Hypothalamic Regulation of Liver and Muscle Nutrient Partitioning by Brain-Specific Carnitine Palmitoyltransferase 1C in Male Mice

Macarena Pozo,[1] Rosalía Rodríguez-Rodríguez,[1] Sara Ramírez,[1] Patricia Seoane-Collazo,[2] Miguel López,[2,3] Dolors Serra,[3,4] Laura Herrero,[3,4] and Núria Casals[1,3]

[1]Basic Sciences Department, Faculty of Medicine and Health Sciences, Universitat Internacional de Catalunya, 08195 Sant Cugat del Vallès, Barcelona, Spain; [2]NeurObesity Group, Department of Physiology, CIMUS, University of Santiago de Compostela-Instituto de Investigación Sanitaria, 15782 Santiago de Compostela, Spain; [3]Centro de Investigación Biomédica en Red de Fisiopatología de la Obesidad y la Nutrición (CIBEROBN), Instituto de Salud Carlos III, 28029 Madrid, Spain; and [4]Department of Biochemistry and Physiology, Faculty of Pharmacy, Institut de Biomedicina de la Universitat de Barcelona, Universitat de Barcelona, 08028 Barcelona, Spain

Carnitine palmitoyltransferase (CPT) 1C, a brain-specific protein localized in the endoplasmic reticulum of neurons, is expressed in almost all brain regions. Based on global knockout (KO) models, CPT1C has demonstrated relevance in hippocampus-dependent spatial learning and in hypothalamic regulation of energy balance. Specifically, it has been shown that CPT1C is protective against high-fat diet–induced obesity (DIO), and that CPT1C KO mice show reduced peripheral fatty acid oxidation (FAO) during both fasting and DIO. However, the mechanisms mediating CPT1C-dependent regulation of energy homeostasis remain unclear. Here, we focus on the mechanistic understanding of hypothalamic CPT1C on the regulation of fuel selection in liver and muscle of male mice during energy deprivation situations, such as fasting. In CPT1C-deficient mice, modulation of the main hypothalamic energy sensors (5′ adenosine monophosphate-activated protein kinase, Sirtuin 1, and mammalian target of rapamycin) was impaired and plasma catecholamine levels were decreased. Consequently, CPT1C-deficient mice presented defective fasting-induced FAO in liver, leading to higher triacylglycerol accumulation and lower glycogen levels. Moreover, muscle pyruvate dehydrogenase activity was increased, which was indicative of glycolysis enhancement. The respiratory quotient did not decrease in CPT1C KO mice after 48 hours of fasting, confirming a defective switch on fuel substrate selection under hypoglycemia. Phenotype reversion studies identified the mediobasal hypothalamus (MBH) as the main area mediating CPT1C effects on fuel selection. Overall, our data demonstrate that CPT1C in the MBH is necessary for proper hypothalamic sensing of a negative energy balance and fuel partitioning in liver and muscle. (***Endocrinology*** **158: 2226–2238, 2017)**

The hypothalamus plays a central role in energy balance regulation in mammals because it integrates the metabolic status of the organism through metabolite, hormone, and nutrient sensing. Several studies have clearly shown the involvement of hypothalamic lipid metabolism in regulation of food intake and energy homeostasis (1). Among the different lipid players, it is important to mention carnitine palmitoyltransferase

ISSN Print 0013-7227 ISSN Online 1945-7170
Printed in USA

Received 10 February 2017. Accepted 28 April 2017.
First Published Online 3 May 2017

Abbreviations: AMPK, adenosine monophosphate–activated protein kinase; CPT, carnitine palmitoyltransferase; DIO, high-fat diet–induced obesity; eWAT, epididymal white adipose tissue; FAO, fatty acid oxidation; GFP, green fluorescence protein; HRP, horseradish peroxidase; KO, knockout; LCFA, long-chain fatty acid; MBH, mediobasal hypothalamus; mTOR, mammalian target of rapamycin; NEFA, nonesterified fatty acid; PCR, polymerase chain reaction; PDH, pyruvate dehydrogenase; PDK4, pyruvate dehydrogenase 4; PEPCK, phosphoenolpyruvate carboxykinase; RQ, respiratory quotient; RRID, Research Resource Identifier; SEM, standard error of the mean; Sirt1, Sirtuin 1; TAG, tissue triacylglycerol; UCP2, uncoupling protein 2; WT, wild-type; w/v, weight-to-volume ratio.

(CPT) 1 enzymes, malonyl-CoA, long-chain fatty acids (LCFAs), ceramides, uncoupling protein 2 (UCP2), or lipoprotein lipase (2–11). Most of these molecules are downstream factors of 5′ adenosine monophosphate–activated protein kinase (AMPK), a hypothalamic key energy sensor that responds to peripheral hormones and to food scarcity to preserve appetite and regulate peripheral metabolism (12–14).

In this study, we focused on the role of hypothalamic CPT1C in the regulation of fuel selection by peripheral tissues during fasting. CPT1C is a downstream factor of AMPK, whose expression levels increase in response to AMPK activation (15). Contrary to the other CPT1 isoforms (*i.e.*, CPT1A and CPT1B), CPT1C is located in the endoplasmic reticulum of neurons instead of the outer membrane of mitochondria, and has negligible CPT1 activity (16, 17). However, it is able to bind malonyl-CoA and LCFA-CoAs with similar affinities than CPT1A (16, 18, 19), suggesting that it might act as a sensor of these lipid intermediaries in hypothalamus (8). In fact, it has been involved in hypothalamic leptin and ghrelin signaling pathways in the control food intake (20, 21). Moreover, its deletion reduces peripheral fatty acid oxidation (FAO) induction in response to high-fat diet or fasting, leading to an obesogenic phenotype (19, 22, 23). However, the molecular and physiological mechanisms leading to those effects are completely unknown.

Here, we describe the metabolic inflexibility shown by CPT1C knockout (KO) mice in response to changes in nutrient availability. Specifically, we focus on the metabolic parameters and signaling pathways in the hypothalamus, plasma, liver, and muscle of CPT1C KO mice during fasting. Our results show that CPT1C-deficient mice exhibit a continuous fed-like hypothalamic energy sensor status during food deprivation, resulting in decreased plasma catecholamine levels and impaired hepatic and muscular fuel partitioning. Moreover, we identify the mediobasal hypothalamus (MBH) as the area of CPT1C function responsible for these effects.

Materials and Methods

Animals

We used 8- to 10-week-old male CPT1C KO mice (24) in a C57BL/6J background. They were housed in a controlled environment (*i.e.*, 12 hours of light and 12 hours of dark) with free access to food and water. For fasting experiments, animals were either food-deprived 1 hour after beginning the light cycle (09:00) for a total of 24 hours (fasted) or fed *ad libitum* (fed). After this period, they were euthanized by cervical dislocation. MBH, liver, muscle (gastrocnemius), and epididymal white adipose tissue (eWAT) were dissected and stored at −80°C. To dissect the MBH, brains were placed in a coronal brain matrix (Roboz Surgical Instrument, Gaithersburg, MD) and sectioned from bregma (−1 mm to −2.5 mm). Then the MBH was obtained from each section, using a tissue collector measuring 1 mm in diameter. Six- and 48-hour fasting experiments were performed to analyze liver and muscle glycogen stores as well as body weight and glycemia. Animal procedures were carried out in accordance with Spanish legislation (BOE 32/2007), EU Directive 2010/63/EU for animal experiments, and were approved by the local ethics committee.

Indirect calorimetry, locomotor activity, and body composition analysis

Mice were analyzed for energy expenditure, respiratory quotient (RQ), and locomotor activity using a calorimetric system (LabMaster; TSE Systems, Bad Homburg, Germany), as previously shown (25–27). Mice were placed for adaptation for 1 week before starting the measurements. For the measurement of body composition, we used nuclear magnetic resonance imaging (Whole Body Composition Analyzer; EchoMRI, Houston, TX), as previously shown (28, 29). We used six animals per experimental group.

Lentivirus production and hypothalamic delivery

Two lentiviral vectors, pWPI-IRES-GFP and pWPI-CPT1C-IRES-GFP, were constructed to drive the expression of green fluorescence protein (GFP) and CPT1C plus GFP, respectively. The map and sequences of these plasmids are available at Addgene (Cambridge, MA). Lentiviruses were propagated and titrated as previously described (30). Stereotaxic surgery to target the MBH was performed under ketamine/xylazine anesthesia. Mice were injected with lentivirus particles (1×10^9 pfu/mL; 500 nL/side over 10 minutes; injection rate, 50 nL/min) using a Hamilton syringe (catalog no. 65460-02; Hamilton Robotics, Bonaduz, Switzerland). The coordinates used from bregma were as follows: anterior/posterior, −1.5; lateral, ±0.4; dorsal/ventral, −5.8. Mice underwent 1 week of recovery before other experiments were performed. Correct bilateral MBH infection was confirmed histologically by GFP fluorescence in brain sections.

Pyruvate tolerance test

Pyruvate (2 g/kg; Sigma-Aldrich, Madrid, Spain) was administered intraperitoneally after 15 hours of fasting. Blood samples were collected from the tail vein and glucose concentrations were measured using a Glucometer Elite (Bayer, Barcelona, Spain) at baseline and at the indicated times after intraperitoneal administration.

Tissue triacylglycerol and glycogen quantification

For tissue triacylglycerol (TAG) and glycogen quantification, pulverized frozen tissue (≈100 mg) was homogenized in 500 μL of phosphate-buffered saline. Lipids were extracted using chloroform, dried under a N_2 stream, and redissolved in *n*-propanol. TAGs were quantified using the Triglycerides Determination Kit (Linear Chemicals, Barcelona, Spain). Glycogen extraction and quantification were performed as previously described (31) after 6 hours of fasting, with minor modifications. Briefly, muscle or liver tissue (≈100 mg) was homogenized with 250 μL of potassium hydroxide 30% [weight-to-volume ratio (w/v)] and digested at 95°C for 15 minutes. Then 120 μL of homogenate was placed on 2 × 2 cm Whatman filter paper and dried before adding 66% cold ethanol (volume-to-volume ratio) for glycogen precipitation. After three washes with ethanol,

filters were dried again and incubated with 1 mL of glycogen digestion solution (0.5 mg/mL of amyloglucosidase in 400 mM sodium acetate at pH 4.8) at 37°C for 90 minutes to hydrolyze glycogen into glucose monomers. Glucose samples were quantified using the Glucose Determination Kit (Linear Chemicals, Barcelona, Spain).

Plasma metabolite analysis

Catecholamine levels in plasma were measured in fed and fasting conditions using a 2-CAT Research enzyme-linked immunosorbent assay kit (Labor Diagnostica Nord, Nordhorn, Germany) following the manufacturer's instructions. TAG and nonesterified fatty acids (NEFAs) were determined by a triglyceride kit (Sigma-Aldrich, Madrid, Spain) and NEFA-HR detection kit (Wako Diagnostics, Richmond, VA), respectively.

Pyruvate dehydrogenase activity assay

Pyruvate dehydrogenase (PDH) activity was measured using a Microplate Assay Kit (Abcam, Cambridge, UK). PDH was immunocaptured in the microplate and activity was determined by following the reduction of NAD^+ to NADH coupled to a reduction in a reporter dye, the concentration of which could be monitored by absorbance at 450 nm. Muscle tissue (≈50 mg) was homogenized in phosphate-buffered saline in the presence of protease, phosphatase, and kinase inhibitors. Samples were then solubilized and diluted according to the manufacturer's instructions, the reaction mixture was added, and absorbance was recorded at 30°C every minute for 15 minutes.

RNA extraction and real-time polymerase chain reaction

Total RNA was extracted using Trizol reagent (Fisher Scientific, Madrid, Spain) according to the manufacturer's recommendations. For gene expression analysis, template cDNA was obtained from 1 μg of total RNA by reverse transcription using Moloney−Murine Leukemia Virus (M-MLV) reverse transcription and random primers (Fisher Scientific, Madrid, Spain). Of the reaction, 1/20 was used with the polymerase chain reaction (PCR) mix SsoAdvanced SYBRGreen Supermix (BioRad, Madrid, Spain) for quantitative real-time PCR (CFX96 Real-time System; BioRad, Madrid, Spain). The following gene-specific intron-skipping primers (IDT DNA Technologies, Leuven, Belgium) were used: *CPT1C* (*for*-TATGCAGTCGCCCTTCCT, *rev*-ACATCAATCAGGTGTGTCTGCT); *UCP2 (for*-GCTCAGCACAGTTGACAATG, *rev*-CCTACAAGACCATTGCACGA); pyruvate dehydrogenase 4 (*PDK4 for*-CGCTTAGTGAACACTCCTTCG, *rev*-CTTCTGGGCTCTTCTCATGG); phosphoenolpyruvate carboxykinase (*PEPCK; for*-GATGACATTGCCTGGATGAA, *rev*-AACCGTTTTCTGGGTTGATG); *CPT1B* (*for*-TGCCTTTACATCGTCTCCAA, *rev*-GGCTCCAGGGTTCAGAAAGT), and glyceraldehyde 3-phosphate dehydrogenase (*for*-TCCACTTTGCCACTGCA, *rev*-GAGACGGCCGCATCTTCTT). Relative gene expression was estimated using the comparative Ct (2-ΔΔct) method in relation to glyceraldehyde 3-phosphate dehydrogenase levels.

Western blot analysis

Tissue was homogenized in radioimmunoprecipitation assay buffer (Sigma-Aldrich) containing protease and phosphatase inhibitor cocktails. Liver and muscle were homogenized using the Fast-Prep-24 homogenizer (MP Biomedicals, Santa Ana, CA) and the MBH was sonicated. Next, protein extracts were separated on sodium dodecyl sulfate polyacrylamide gels (Criterion Precast Gel; BioRad) and then transferred into Immobilion-P PVDF membranes (Merck Millipore, Madrid, Spain). Blots were blocked with 5% (w/v) dry milk in Tris-buffered saline with Tween 20 and incubated overnight at 4°C with the following primary antibodies in Tween 20 with 0.2% (w/v) bovine serum albumin: Sirtuin 1 [Sirt1; catalog no. 07-131, Research Resource Identifier (RRID): AB_11214517; Merck Millipore], pAMPK (catalog no. 2535, RRID: AB_331250; Cell Signaling, Danvers, MA), mammalian target of rapamycin (mTOR) and phospho-mTOR (catalog no. 2972 and 2971, RRID: AB_330978 and AB_330970, respectively; Cell Signaling), CPT1A (32), CPT1C (16), and β-actin (catalog no. ma1-91399, RRID: AB_2273656; Fisher Scientific). After washing, blots were incubated with horseradish peroxidase (HRP)-conjugated secondary antibodies [anti-mouse immunoglobulin M (IgM) HRP and anti-rabbit IgG HRP, RRID: AB_258413 and AB_390191, respectively)] and developed using LuminataForte Western HRP substrate (Merck Millipore). Semiquantitative analysis was performed using densitometry GeneTools software (Syngene, Cambridge, UK), and β-actin was used as an endogenous control to normalize protein expression levels.

Statistical analysis

Data are expressed as mean ± standard error of the mean (SEM). Statistical analysis of differences was performed using GraphPad Prism Software (GraphPad Software, La Jolla, CA). The two-way analysis of variance test was used to analyze the effects of two different independent variables (the genotype and the feeding status), followed by *post hoc* analysis. Experiments in which data were repeatedly collected over time were analyzed by repeated measures of analysis of variance. For all analyses, significant values were set at $P < 0.05$.

Results

CPT1C KO mice show impaired regulation of hypothalamic energy and nutrient sensors in response to fasting

We first analyzed the expression of CPT1C in the MBH and in the whole hypothalamus. Notably, CPT1C expression in the MBH was increased after 24 hours of fasting in wild-type (WT) mice [Fig. 1(a)], suggesting a role for CPT1C in this hypothalamic area when nutrient availability is compromised. Then we analyzed the expression or phosphorylation grade of several relevant energy metabolic markers in the MBH of CPT1C KO and WT mice during the fed-to-fast transition. Fasting is known to trigger activation of the energy sensor AMPK in the hypothalamus (33, 34). As expected, phosphorylated AMPK levels increased after 24 hours of fasting in WT mice [Fig. 1(b)]. By contrast, CPT1C KO mice showed increased pAMPK levels in the fed state, which were decreased after fasting [Fig. 1(b)].

Because AMPK promotes FAO at the cellular level, we analyzed the expression of UCP2, which is activated

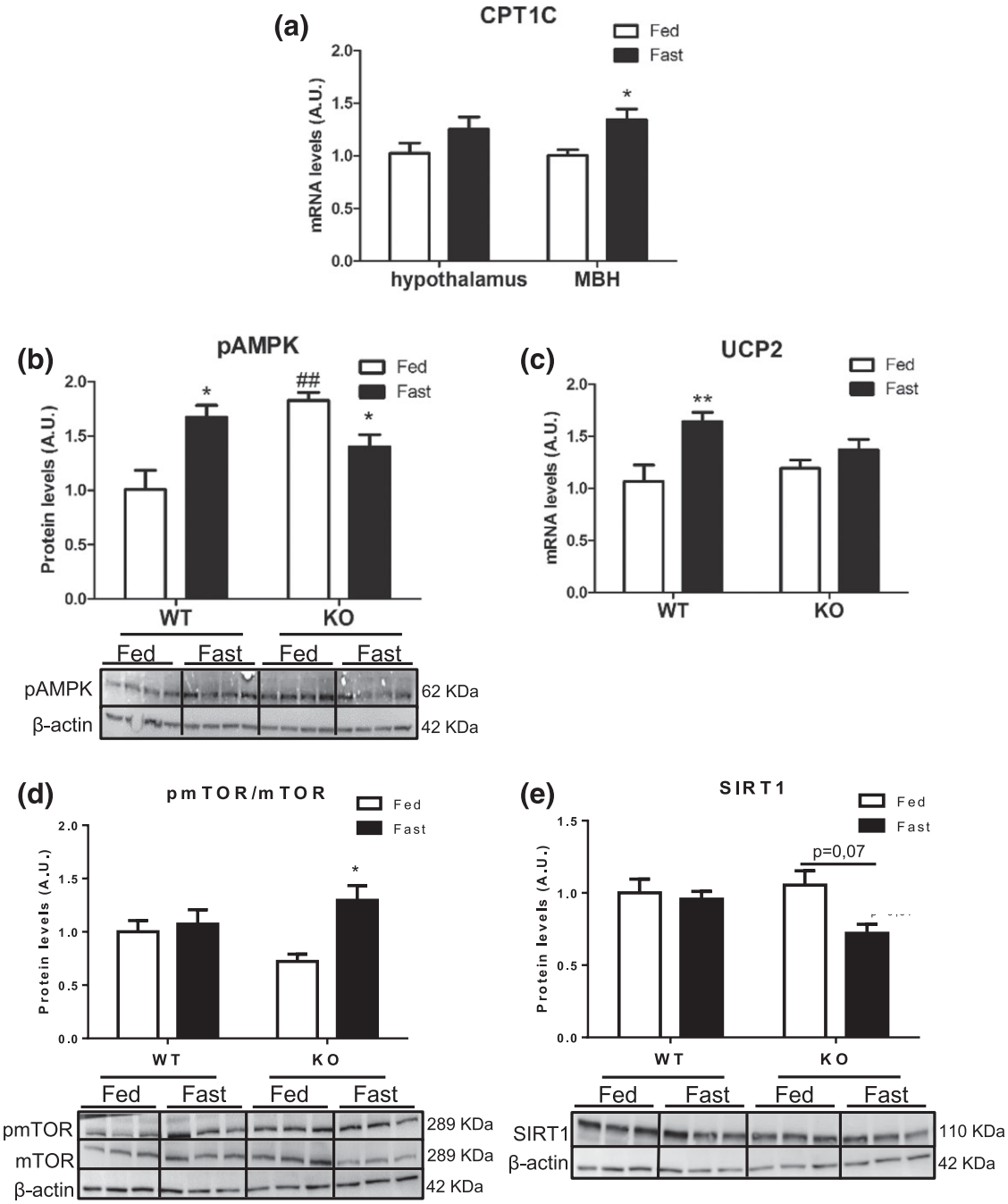

Figure 1. Hypothalamic energy sensors are disrupted in CPT1C KO mice in response to 24 hours of fasting. (a) CPT1C mRNA levels in MBH and whole hypothalamus of WT mice. Protein levels of (b) pAMPK, (d) pmTOR, and (e) Sirt1 were measured by Western blot in MBH of WT and CPT1C KO mice. (c) UCP2 mRNA expression levels were measured by real-time PCR. Results are represented as mean ± SEM (n = 6 to 8). $^{*}P < 0.05$, $^{**}P < 0.01$ relative to fed state within the same genotype; $^{\#}P < 0.05$, $^{\#\#}P < 0.01$ relative to WT under the same diet conditions. A.U., arbitrary unit.

to regulate mitochondrial reactive oxygen species derived from FAO. Consistent with the pAMPK levels, the fasting-induced UCP2 rise was completely abolished in CPT1C KO mice [Fig. 1(c)]. Moreover, in the MBH of fasted CPT1C KO mice, mTOR, a sensor of nutrient availability (35, 36), showed a higher rate of phosphorylation [*i.e.* activation; Fig. 1(d)] than in WT mice. The expression of Sirt1, a NAD^{+}-dependent deacetylase that is a key mediator of the central response to low nutritional availability (37), showed a tendency to be decreased in CPT1C KO mice during fasting compared with the fed state [Fig. 1(e)], whereas it did not change in WT mice. These results combined suggest that CPT1C deficiency causes dysregulation of nutrient- and energy-sensing markers in MBH in response to fasting.

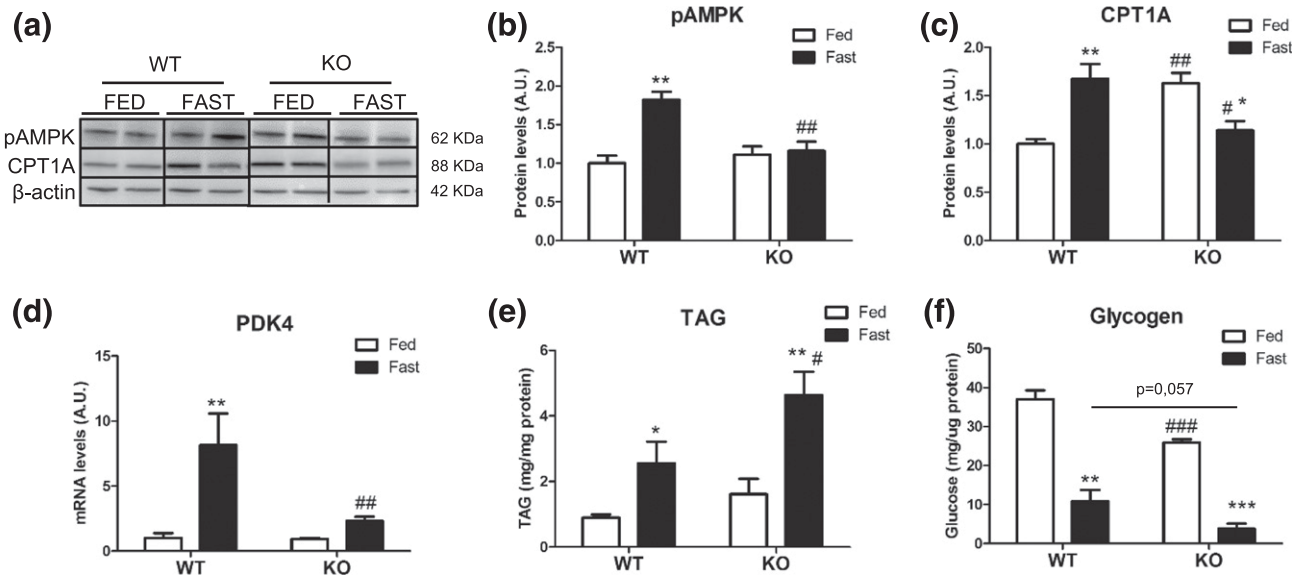

Figure 2. Impaired liver nutrient partitioning in CPT1C KO mice. (a) A representative Western blot analysis of pAMPK and CPT1A expression in liver homogenates from WT and CPT1C KO mice. Quantification of (b) pAMPK and (c) CPT1C protein expression levels. (d) Nutrient switch metabolism was measured by mRNA levels of PDK4 quantified from total RNA extracts. (e) Hepatic TAG and (f) glycogen content of fed and fasted WT and CPT1C KO mice. Results are represented as mean ± SEM (n = 6 to 8). $^{*}P < 0.05$, $^{**}P < 0.01$, $^{***}P < 0.005$ relative to fed state within the same genotype; $^{\#}P < 0.05$, $^{\#\#}P < 0.01$, $^{\#\#\#}P < 0.005$ relative to WT under the same diet conditions. A.U., arbitrary unit.

Fasting-induced liver FAO is impaired in CPT1C KO mice

At the peripheral level, AMPK is an important energy sensor that contributes to activating FAO during glucose scarcity. AMPK induces the expression of CPT1A, which facilitates the entrance of LCFAs into mitochondria for their β-oxidation, and PDK4, which phosphorylates and inhibits PDH enzyme. Consequently, FAO is activated and pyruvate oxidation is inhibited, allowing the utilization of the pyruvate surplus as gluconeogenic substrate. We found that liver pAMPK levels were increased in WT mice fasted for 24 hours, whereas this rise was blunted in CPT1C KO mice [Fig. 2(a) and 2(b)]. Moreover, livers from CPT1C KO mice showed decreased levels of CPT1A and PDK4 after fasting when compared with WT mice [Fig. 2(c) and 2(d)], indicating that FAO induction was impaired and glucose-derived pyruvate oxidation was prevalent over FAO. In keeping with this, CPT1C KO mice exhibited elevated TAG levels after 24 hours of fasting [Fig. 2(e)], and almost complete glycogen depletion after 6 hours of fasting [Fig. 2(f)]. These findings are suggestive that the switch in fuel substrate use in the liver is not properly activated in CPT1C KO mice.

CPT1C KO mice show defective muscle FAO activation during fasting

A similar pattern to liver-defective nutrient partitioning was observed in the gastrocnemius muscle of CPT1C KO mice. AMPK showed a tendency to be activated in WT mice during fasting, but this effect was not observed in CPT1C KO mice [Fig. 3(a)]. Moreover, a significant induction of CPT1B expression was not observed [Fig. 3(b)]. More interestingly, PDH activity in muscle homogenates from fasted CPT1C KO mice was induced instead of inhibited [Fig. 3(c)]. These results indicate that nutrient partitioning is also impaired in the muscle of these mice, which continues to use glucose-derived pyruvate as fuel, instead of switching the energetic substrate to fatty acids. Remarkably, muscle glycogen content declined at the same rate in WT and KO mice during fasting [Fig. 3(d)], suggesting that the circulating glucose was the fuel used to feed muscle PDH activity.

CPT1C KO mice show increased hepatic gluconeogenesis but normal fasting glycaemia

Because results reported thus far for this study indicated that the liver and muscle of CPT1C KO mice keep using glucose as fuel substrate during food deprivation, we analyzed whether CPT1C KO mice had more severe hypoglycemia than WT mice after 48 hours of fasting. Our results showed that both genotypes had the same blood glucose levels after long fasting [Fig. 4(a)], demonstrating an accurate control of glycemia by CPT1C KO mice. We then explored whether liver gluconeogenesis was increased to counteract muscular glucose use. Liver PEPCK mRNA levels (a well-established gluconeogenesis marker) were higher in fasted CPT1C KO mice than in WT mice [Fig. 4(b)]. In addition, we performed a pyruvate tolerance test to overnight fasted animals and found that blood glucose levels after pyruvate administration were higher in CPT1C KO mice than in WT mice, confirming the major

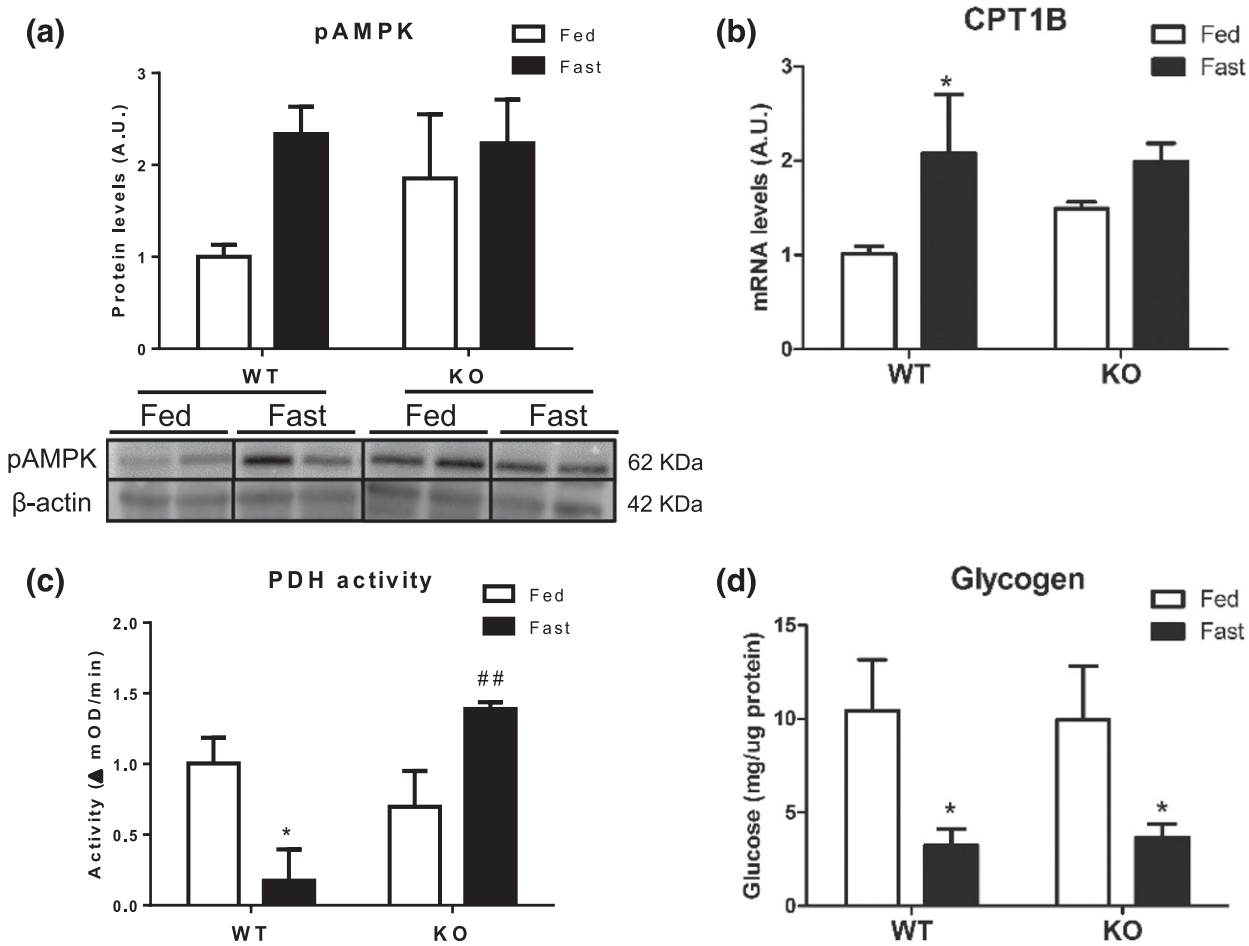

Figure 3. Impaired muscle nutrient partitioning in CPT1C KO mice. (a) Gastrocnemius muscle was isolated from WT and CPT1C KO mice to measure pAMPK protein levels, (b) CPT1B mRNA levels, (c) PDH activity, and (d) glycogen content. Results are represented as mean ± SEM (n = 6 to 8). $^{*}P < 0.05$ relative to fed state within the same genotype; $^{\#\#}P < 0.01$ relative to WT under the same diet conditions. A.U., arbitrary unit.

increase in hepatic gluconeogenesis in CPT1C-deficient mice during fasting [Fig. 4(c)]. Overall, these data indicate that although the liver of CPT1C KO fails to switch fuel use from glucose to fatty acids, it is able to adapt the gluconeogenesis rate for a precise control of blood glucose levels.

Fasting-induced decrease in adiposity is attenuated in CPT1C KO mice

Because CPT1C KO mice present a defect in liver and muscle use of lipids, we next analyzed whether lipid mobilization from fat stores was affected. The fasting-induced reduction of eWAT was lower in CPT1C KO mice than in WT mice [WT: 60% vs KO: 34%;Fig. 5(a)], which is consistent with lower use of fatty acids as fuel by peripheral tissues. Accordingly, CPT1C KO mice displayed resistance to losing weight after 48 hours of fasting [Fig. 5(b)]. Interestingly, CPT1C KO mice exhibited decreased plasma norepinephrine levels after fasting compared with control mice [Fig. 5(c)], which could partially explain the reduced mobilization of fats. We also measured plasma NEFA and TAG and found no differences between the genotypes [Fig. 5(d)]. In both genotypes, NEFA levels were increased and TAG levels were reduced at fasting, as expected for the WT mice. This suggests that the reduced delivery of NEFA from eWAT in CPT1C KO mice at fasting is counteracted by the lower FAO in liver and muscle.

The inability of CPT1C KO mice to properly use fatty acids as fuel appeared to have long-term consequences. CPT1C KO mice showed higher adiposity and lower lean mass than WT mice [Fig. 5(e)]. In addition to reshaped body composition, CPT1C KO mice presented higher body weight gain with age [Fig. 5(f)], which was independent of food intake [Fig. 5(g)].

Finally, to confirm that CPT1C-deficient mice do not properly switch fuel substrate at fasting, we performed indirect calorimetry under *ad libitum* fed and fasted conditions. Results showed that the RQ (CO_2 production divided by oxygen consumption) of WT mice decreased at fasting, whereas it remained unaffected in CPT1C KO mice [Fig. 5(h)], confirming the incapacity of those mice to promote liver and muscle FAO under food deprivation. Notably, no differences were observed in energy expenditure

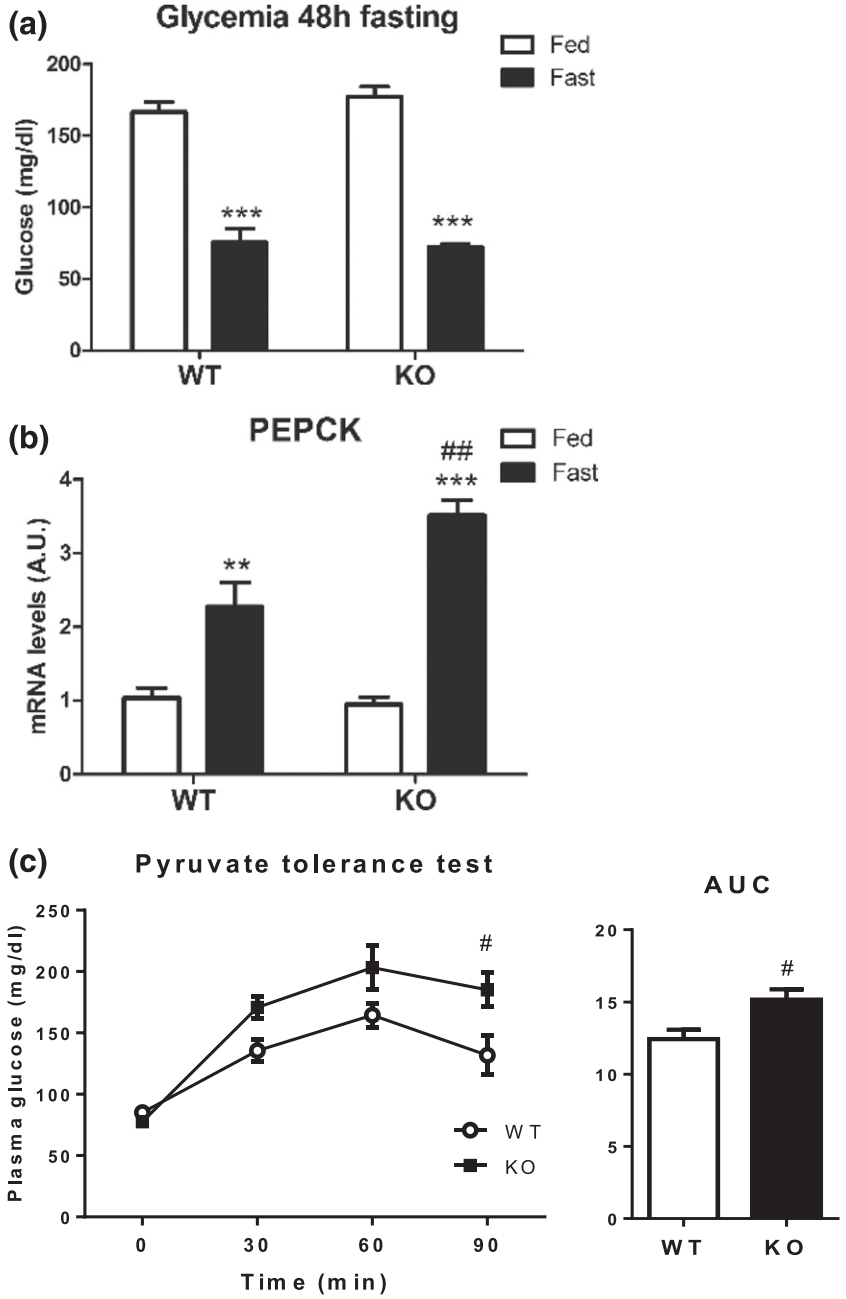

Figure 4. (a) Glucose homeostasis in WT and CPT1C KO mice. Glycemia after 48 hours of fasting is indicated. (b) PEPCK mRNA levels were determined by quantitative PCR analysis. (c) A pyruvate tolerance test was performed in WT and CPT1C KO mice after an overnight fast; plasma glucose levels and AUC are represented. Results are represented as mean ± standard error of the mean (SEM; n = 6 to 8). $^{*}P < 0.05$, $^{**}P < 0.01$, $^{***}P < 0.005$ relative to fed state within the same genotype; $^{\#\#}P < 0.01$ relative to WT under the same diet conditions. A.U., arbitrary unit; AUC, area under the curve.

(Supplemental Fig. 1) and locomotor activity (Supplemental Fig. 2) either in light or dark phase in CPT1C KO mice compared with control animals.

CPT1C overexpression specifically in the MBH is sufficient to reverse the metabolic phenotype of CPT1C KO mice

To further confirm the involvement of CPT1C in peripheral metabolic regulation, we specifically expressed CPT1C in the MBH of CPT1C KO mice through bilateral and intraparenchyma stereotaxic injection of lentivirus harboring CPT1C [the experimental timing diagram is shown in Fig. 6(a)]. Overexpression of CPT1C in the MBH was assessed by the presence of fluorescence in the histological sections [Fig. 6(b)]. Western blot analysis of MBH punches revealed that CPT1C KO mice injected with CPT1C-GFP harboring viruses expressed 66.9% ± 1.4% levels of CPT1C with respect to WT mice injected with GFP viruses [Fig. 6(c)]. Overexpression of CPT1C ameliorated the defects in nutrient partitioning in liver and muscle, as evidenced by the restored response in liver PDK4 levels [Fig. 6(d)] and the trend in muscle

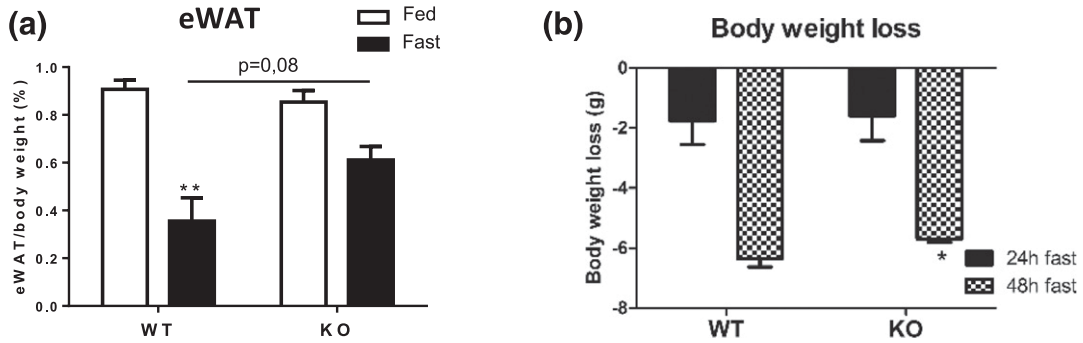

(c)

Plasma catecholamines (pg/ml)

	Controls		CPT1C-KO	
	Fed	Fast	Fed	Fast
Epi	11,315 ± 3,389	28,732 ± 11,423 **	11,259 ± 5,973	23,636 ± 6,173 *
Norepi	12,802 ± 2,712	35,008 ± 6.588 **	16,401 ± 3,364	25,651 ± 8.346 #

(d)

Plasma Lipid Profile

	Controls		CPT1C-KO	
	Fed	Fast	Fed	Fast
NEFA (mM)	0,688 ± 0,03	0,958 ± 0,02*	0,706 ± 0,04	0,967 ± 0,11*
TAG (mM)	1,609 ± 0,14	0,727 ± 0,07***	1,338 ± 0,08	0,689 ± 0,15***

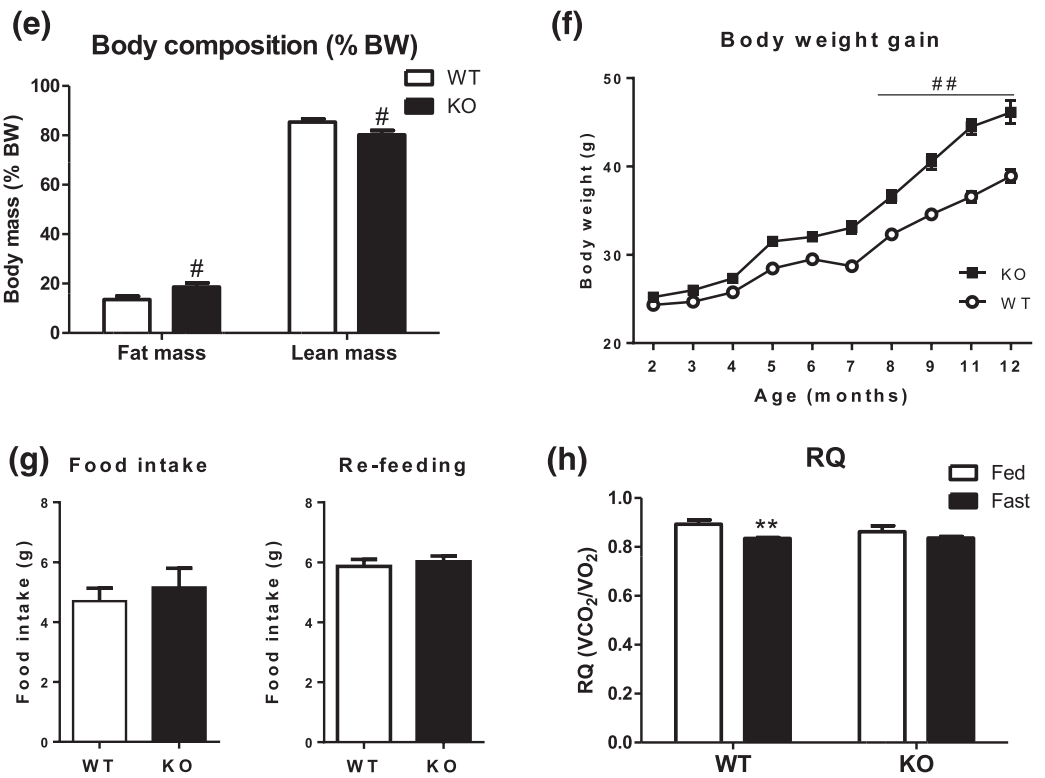

Figure 5. Adiposity, plasma catecholamine levels, and RQ in WT and CPT1C KO mice. (a) eWAT tissue was weighed in fed and 24-hour fasted animals. (b) Body weight was measured after 24 and 48 hours of fasting. (c) Plasma catecholamine levels in fed and 24-hour fasted animals. (d) NEFA and TAG levels in fed and 24-hour fasted mice. (e) Body mass composition was measured by nuclear magnetic resonance imaging. (f) Body weight gain and (g) 24-hour food intake were monitored monthly until animals reached 12 months of age. Refeeding was calculated as 24-hour food intake after 24 hours of fasting, at 10 months of age. RQ was measured by indirect calorimetry. (h) Mice were maintained 48 hours at normal conditions and 48 hours under fasting. Results are represented as mean ± SEM (n = 6 to 8). $^{*}P < 0.05$, $^{**}P < 0.01$, $^{***}P < 0.005$ relative to fed state within the same genotype; $^{\#}P < 0.05$ relative to WT under the same diet conditions. Epi, epinephrine; Norepi, norepinephrine.

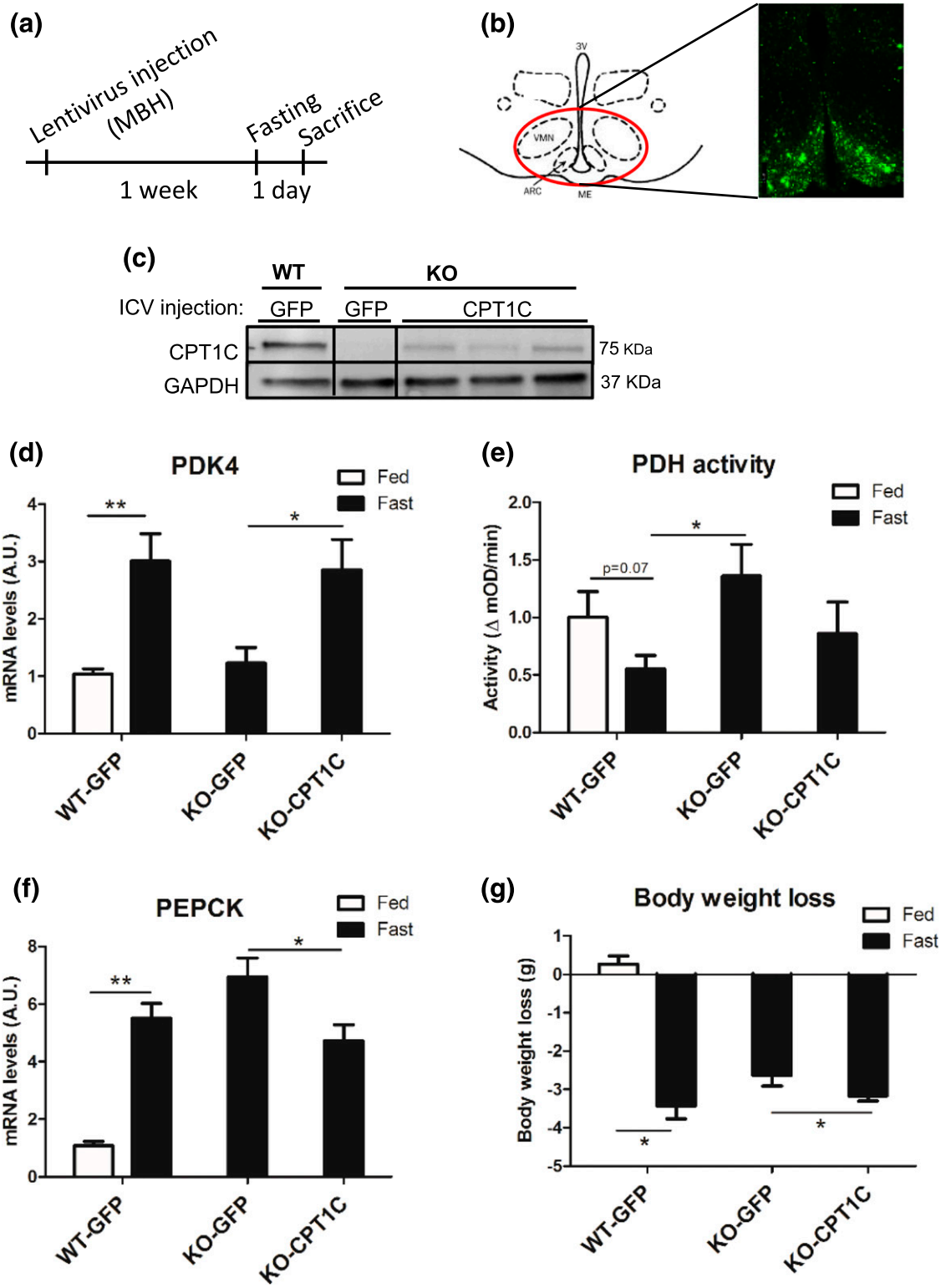

Figure 6. MBH-specific overexpression of CPT1C reverses the fasting phenotype of CPT1C KO mice. (a) GFP or CPT1C-GFP expressing lentiviruses were microinjected bilaterally in the MBH of WT and CPT1C KO mice, and 1 week later were exposed to 24-hour fasting. Half of the mice group was used to confirm the proper injection site by histological analysis, and the other half to analyze CPT1C expression in MBH by Western blot. (b) A representative image of GFP fluorescence photomicrograph of virus expression localization in the MBH region is shown. (c) Western blot analysis. (d) Liver PDK4 mRNA levels, (e) muscle PDH activity, and (f) liver PEPCK mRNA levels are shown. (g) Body weight loss is indicated. Results are represented as mean ± SEM (n = 5 to 6). $*P < 0.05$, $**P < 0.01$. A.U., arbitrary unit.

PDH activity to be reduced [Fig. 6(e)]. In accordance with a re-established fuel tunneling, liver PEPCK mRNA levels were decreased, indicative of a restored liver gluconeogenesis [Fig. 6(f)]. Moreover, all these responses where associated to normalization of the fasting-induced body weight loss [Fig. 6(g)].

Discussion

In this study, we demonstrate the mechanisms by which hypothalamic CPT1C regulates hepatic and muscular key enzymes involved in nutrient partitioning during negative energy balance, such as fasting. Fuel use of fat stores over carbohydrates in peripheral tissues is a crucial metabolic adaptation to preserve plasma glucose for brain metabolism, avoiding fainting and, hence, maintaining appropriated cognitive functions during fasting.

First, we demonstrated that CPT1C expression is triggered by fasting in the MBH, a hypothalamic area containing glucose and fatty-acid–sensing neurons (38, 39) and closely related to peripheral metabolism regulation (40, 41), suggesting a key role of CPT1C in nutrient-scarce conditions. Here, we showed that CPT1C deficiency completely blunts the canonical AMPK-UCP2 pathway in MBH, which ought to be activated during fasting (42, 43). Hypothalamic AMPK drives the shift from negative to neutral energy balance (14), and UCP2 in agouti-related protein/Neuropeptide Y neurons promotes FAO over glucose use during food deprivation (44, 45), so its impairment in CPT1C KO mice can account for the metabolic inflexibility of these mice. Moreover, the energy markers Sirt1 and mTOR did not respond properly to changes in nutrient availability in the MBH of CPT1C-deficient mice, confirming the involvement of CPT1C in hypothalamic sensing of nutrient deprivation. On the other hand, recent observations suggest that synaptic plasticity is a component in the hypothalamic control of energy homeostasis (46–49). CPT1C has been demonstrated to regulate the trafficking of AMPA-type glutamate receptors and dendritic spinogenesis (24, 50–53); therefore, further work will be worthwhile to address the putative role of CPT1C in hypothalamic synaptic plasticity.

At the peripheral level, fasting does not properly activate the autonomous nervous system in CPT1C KO mice, resulting in decreased plasma catecholamine levels, which may be the cause, at least partially, of impaired responses of liver and muscle to fasting. In liver, CPT1C KO mice show a clear deregulation of the AMPK-CPT1A axis (FAO enhancers), and the AMPK downstream factor PDK4, which is a key kinase responsible for switching nutrient use from carbohydrates to fatty acids (54, 55). This inability to switch fuel substrates during fasting causes major TAG synthesis and accumulation in the liver, as well as a higher depletion of hepatic glycogen stores in CPT1C KO mice.

The major alteration observed in these mice at the muscular level is a marked activation of PDH activity during fasting, instead of the inhibition observed in WT mice. PDH activity together with PDK4 expression are crucial in nutrient partitioning in muscle (56). The inappropriate suppression of PDH activity and the major pyruvate-derived tricarboxylic flux should produce a major decrease in muscle glycogen stores in CPT1C-deficient mice; however, that was not the case, suggesting that those mice were using blood glucose as the main substrate. Meanwhile, fasting blood glucose in CPT1C KO mice remained exactly the same as in WT mice, probably due to the increased hepatic gluconeogenesis observed. However, we cannot rule out the potential role of proteolysis and amino acid metabolism as an alternative energy source in this context, which could partially contribute to the maintenance of normal glucose levels in CPT1C KO mice.

Results indicate that although CPT1C-deficient mice are unable to properly regulate the peripheral switch in fuel substrate during fasting, they are better able to exert an effective counter-response in glucose production to maintain intact plasma glycemia than are WT mice, indicating that CPT1C is not directly involved in the regulation of glucose homeostasis. Interestingly, the other brain isoform, CPT1A, is involved in the MBH regulation of liver glucose production in response to nutrient signals (4, 5). It seems that the two different CPT1 isoforms in the MBH are regulating different aspects of liver metabolism: counter-response glucose production (by CPT1A) and fuel selection (by CPT1C).

The physiological relevance of these observations is supported by the data from indirect calorimetry, which shows the inability of CPT1C-deficient mice to reduce the RQ (which is indicative of lipid use) after fasting, meaning that these mice continue to use carbohydrates as fuel substrate. As a result of this impairment, CPT1C KO mice exhibit a feeding-independent weight gain and adiposity. Remarkably, low carbohydrate reserves in subjects with low-fat oxidation have been associated with increased weight gain in humans (57), resembling the phenotype of CPT1C deficiency in mice.

Finally, the mechanistic relevance of our data were given by the fact that lentiviral-driven overexpression of CPT1C, specifically in the MBH of CPT1C KO mice, was enough to (1) restore PDK4 and PEPCK expression levels in the liver, (2) reduce muscular PDH activity, and (3) promote effective body weight loss during fasting. Although the experimental model used here was a global CPT1C-deficient mouse, these results are indicative of a key role of CPT1C in MBH.

Appendix. Antibody Table

Peptide/ Protein Target	Antigen Sequence (if Known)	Name of Antibody	Manufacturer, Catalog No., and/or Name of Individual Providing the Antibody	Species Raised in; Monoclonal or Polyclonal	Dilution Used	RRID
Sirt1	Amino acids 1–131 of mouse Sir2α	Anti-Sirt1	Merck Millipore, 07-131	Rabbit; polyclonal	1:2000	AB_11214517
pAMPK	Synthetic peptide corresponding to residues surrounding Thr172 of human AMPKα protein	Phospho-AMPKα (Thr172) (40H9)	Cell Signaling, 2535	Rabbit; monoclonal	1:1000	AB_331250
mTOR	Synthetic peptide corresponding to residues surrounding Ser2481 of human mTOR	mTOR antibody	Cell Signaling, 2972	Rabbit; polyclonal	1:1000	AB_330978
pmTOR	Synthetic phosphopeptide corresponding to residues surrounding Ser2448 of human mTOR	Phospho-mTOR (Ser2448)	Cell Signaling, 2971	Rabbit; polyclonal	1:1000	AB_330970
β-actin	Synthetic peptide DDDIAALVIDNGSGL conjugated to KLH, corresponding to amino acids 1-14 of *Xenopus laevis* actin (β)	*B*-Actin monoclonal antibody (AC-15)	Fisher Scientific, ma1-91399	Mouse; monoclonal	1:5000	AB_2273656
CPT1C	Last 15 amino acids of mouse CPT1C	Anti-CPT1C	NeuroLipid Group/UIC, UIC-ab001	Rabbit; polyclonal	1:5000	AB_2636893
CPT1A	Amino acids 317–430 of rat CPT1A	Anti-CPT1A	Dolors Serra/UB, CPT1A	Rabbit; polyclonal	1:5000	AB_2636894

In summary, this study improves the mechanistic understanding of the CPT1C role in fuel selection of peripheral tissues at fasting and identifies the MBH as the major brain area where CPT1C exerts its effects. These findings highlight the function of CPT1C as a central coordinator of peripheral energy partitioning and confirm CPT1C as a putative target in the treatment of obesity and other related pathologies.

Acknowledgments

Current affiliation: S. Ramírez's current affiliation is Diabetes and Obesity Research Laboratory, Institut d'Investigacions Biomèdiques August Pi i Sunyer (IDIBAPS), 08036 Barcelona, Spain.

Address all correspondence and requests for reprints to: Núria Casals, PhD, Basic Science Department, Facultat de Medicina i Ciències de la Salut, Universitat Internacional de Catalunya, Josep Trueta s/n, 08195 Sant Cugat del Vallés, Spain. E-mail: ncasals@uic.es.

This work was supported by Ministry of Spain Grant SAF2013-45887-R (to L.H.); SAF2014-52223-C2-1-R (to D.S.); SAF2014-52223-C2-2-R (to N.C.); and Grants SAF2015-71026-R and BFU2015-70454-REDT/Adipoplast (to M.L.). All grants were cofunded by Fondos Europeos de Desarrollo Regional de la Unión Europea; Centro de Investigación Biomédica en Red Fisiopatología de la Obesidad y la Nutrición (CIBEROBN) Grant CB06/03/0001 (to D.S.); Generalitat de Catalunya Grant 2014SGR465 (to D.S. and N.C.); European Foundation for the Study of Diabetes/Janssen-Rising Star and L'Oréal-UNESCO "For Women in Science" research fellowships (awarded to L.H.); Fundació La Marató de TV3 Grant 87/C/2016 (to D.S. and N.C.); a Projectes de Recerca per a investigadors novells (2015) grant (to R.R.-R.); the European Community's Seventh Framework Programme (FP7/2007-2013) under Grant Agreement 281854–the ObERStress Project (to M.L.); and Xunta de Galicia Grant 2015-CP079 (to M.L.). M.P. is the recipient of a fellowship from the Agència de Gestió d'Ajuts Universitaris i de la Recerca in Catalonia. CIBER de Fisiopatología de la Obesidad y Nutrición is an initiative of Instituto de Salud Carlos III. The funders had no role in study design, data collection and analysis, decision to publish, or preparation of the manuscript.

Disclosure Summary: The authors have nothing to disclose.

References

1. Blouet C, Schwartz GJ. Hypothalamic nutrient sensing in the control of energy homeostasis. *Behav Brain Res*. 2010;**209**(1): 1–12.

2. He W, Lam TK, Obici S, Rossetti L. Molecular disruption of hypothalamic nutrient sensing induces obesity. *Nat Neurosci*. 2006; **9**(2):227–233.
3. Lam TKT, Schwartz GJ, Rossetti L. Hypothalamic sensing of fatty acids. *Nat Neurosci*. 2005;**8**(5):579–584.
4. Mera P, Mir JF, Fabriàs G, Casas J, Costa ASH, Malandrino MI, Fernández-López JA, Remesar X, Gao S, Chohnan S, Rodríguez-Peña MS, Petry H, Asins G, Hegardt FG, Herrero L, Serra D. Long-term increased carnitine palmitoyltransferase 1A expression in ventromedial hypotalamus causes hyperphagia and alters the hypothalamic lipidomic profile. *PLoS One*. 2014;**9**(5):e97195.
5. Obici S, Feng Z, Arduini A, Conti R, Rossetti L. Inhibition of hypothalamic carnitine palmitoyltransferase-1 decreases food intake and glucose production. *Nat Med*. 2003;**9**(6):756–761.
6. Contreras C, González-García I, Martínez-Sánchez N, Seoane-Collazo P, Jacas J, Morgan DA, Serra D, Gallego R, Gonzalez F, Casals N, Nogueiras R, Rahmouni K, Diéguez C, López M. Central ceramide-induced hypothalamic lipotoxicity and ER stress regulate energy balance. *Cell Reports*. 2014;**9**(1):366–377.
7. Diano S, Horvath TL. Mitochondrial uncoupling protein 2 (UCP2) in glucose and lipid metabolism. *Trends Mol Med*. 2012;**18**(1):52–58.
8. Wolfgang MJ, Lane MD. Hypothalamic malonyl-CoA and CPT1c in the treatment of obesity. *FEBS J*. 2011;**278**(4):552–558.
9. Lane MD, Wolfgang M, Cha S-H, Dai Y. Regulation of food intake and energy expenditure by hypothalamic malonyl-CoA. *Int J Obes*. 2008;**32**(Suppl 4):S49–S54.
10. Shehata M, Matsumura H, Okubo-Suzuki R, Ohkawa N, Inokuchi K. Neuronal stimulation induces autophagy in hippocampal neurons that is involved in ampa receptor degradation after chemical long-term depression. *J Neurosci*. 2012;**32**(30):10413–10422.
11. Kim HK, Shin MS, Youn BS, Kang GM, Gil SY, Lee CH, Choi JH, Lim HS, Yoo HJ, Kim MS. Regulation of energy balance by the hypothalamic lipoprotein lipase regulator angptl3. *Diabetes*. 2015; **64**(4):1142–1153.
12. López M, Varela L, Vazquez MJ, Rodriguez-Cuenca S, Gonzalez CR, Velagapudi VR, Morgan DA, Schoenmakers E, Agassandian K, Lage R, de Morentin PBM, Tovar S, Nogueiras R, Carling D, Lelliott C, Gallego R, Oresic M, Chatterjee K, Saha AK, Rahmouni K, Dieguez C, Vidal-Puig A. Hypothalamic AMPK and fatty acid metabolism mediate thyroid regulation of energy balance. *Nat Med*. 2010;**16**(9):1001–1008.
13. López M, Nogueiras R, Tena-Sempere M, Diéguez C. Hypothalamic AMPK: a canonical regulator of whole-body energy balance. *Nat Rev Endocrinol*. 2016;**12**(7):421–432.
14. Stark R, Ashley SE, Andrews ZB. AMPK and the neuroendocrine regulation of appetite and energy expenditure. *Mol Cell Endocrinol*. 2013;**366**(2):215–223.
15. Zaugg K, Yao Y, Reilly PT, Kannan K, Kiarash R, Mason J, Huang P, Sawyer SK, Fuerth B, Faubert B, Kalliomäki T, Elia A, Luo X, Nadeem V, Bungard D, Yalavarthi S, Growney JD, Wakeham A, Moolani Y, Silvester J, Ten AY, Bakker W, Tsuchihara K, Berger SL, Hill RP, Jones RG, Tsao M, Robinson MO, Thompson CB, Pan G, Mak TW. Carnitine palmitoyltransferase 1C promotes cell survival and tumor growth under conditions of metabolic stress. *Genes Dev*. 2011;**25**(10):1041–1051.
16. Sierra AY, Gratacos E, Carrasco P, Clotet J, Urena J, Serra D, Asins G, Hegardt FG, Casals N. CPT1c is localized in endoplasmic reticulum of neurons and has carnitine palmitoyltransferase activity. *J Biol Chem*. 2008;**283**(11):6878–6885.
17. Casals N, Zammit V, Herrero L, Fadó R, Rodríguez-Rodríguez R, Serra D. Carnitine palmitoyltransferase 1C: from cognition to cancer. *Prog Lipid Res*. 2016;**61**:134–148.
18. Price N, van der Leij F, Jackson V, Corstorphine C, Thomson R, Sorensen A, Zammit V. A novel brain-expressed protein related to carnitine palmitoyltransferase I. *Genomics*. 2002;**80**(4):433–442.
19. Wolfgang MJ, Kurama T, Dai Y, Suwa A, Asaumi M, Matsumoto S, Cha SH, Shimokawa T, Lane MD. The brain-specific carnitine palmitoyltransferase-1c regulates energy homeostasis. *Proc Natl Acad Sci USA*. 2006;**103**(19):7282–7287.
20. Gao S, Zhu G, Gao X, Wu D, Carrasco P, Casals N, Hegardt FG, Moran TH, Lopaschuk GD. Important roles of brain-specific carnitine palmitoyltransferase and ceramide metabolism in leptin hypothalamic control of feeding. *Proc Natl Acad Sci USA*. 2011; **108**(23):9691–9696.
21. Ramirez S, Martins L, Jacas J, Carrasco P, Pozo M, Clotet J, Serra D, Hegardt FG, Dieguez C, Lopez M, Casals N. Hypothalamic ceramide levels regulated by CPT1C mediate the orexigenic effect of ghrelin. *Diabetes*. 2013;**62**(7):2329–2337.
22. Wolfgang MJ, Cha SH, Millington DS, Cline G, Shulman GI, Suwa A, Asaumi M, Kurama T, Shimokawa T, Lane MD. Brain-specific carnitine palmitoyl-transferase-1c: role in CNS fatty acid metabolism, food intake, and body weight. *J Neurochem*. 2008;**105**(4):1550–1559.
23. Gao XF, Chen W, Kong XP, Xu AM, Wang ZG, Sweeney G, Wu D. Enhanced susceptibility of Cpt1c knockout mice to glucose intolerance induced by a high-fat diet involves elevated hepatic gluconeogenesis and decreased skeletal muscle glucose uptake. *Diabetologia*. 2009;**52**(5):912–920.
24. Carrasco P, Sahun I, McDonald J, Ramirez S, Jacas J, Gratacos E, Sierra AY, Serra D, Herrero L, Acker-Palmer A, Hegardt FG, Dierssen M, Casals N. Ceramide levels regulated by carnitine palmitoyltransferase 1C control dendritic spine maturation and cognition. *J Biol Chem*. 2012;**287**(25):21224–21232.
25. Imbernon M, Beiroa D, Vázquez MJ, Morgan DA, Veyrat-Durebex C, Porteiro B, Díaz-Arteaga A, Senra A, Busquets S, Velásquez DA, Al-Massadi O, Varela L, Gándara M, López-Soriano F-J, Gallego R, Seoane LM, Argiles JM, López M, Davis RJ, Sabio G, Rohner-Jeanrenaud F, Rahmouni K, Dieguez C, Nogueiras R. Central melanin-concentrating hormone influences liver and adipose metabolism via specific hypothalamic nuclei and efferent autonomic/JNK1 pathways. *Gastroenterology*. 2013;**144**(3):636–649.e6.
26. Nogueiras R, Wiedmer P, Perez-Tilve D, Veyrat-Durebex C, Keogh JM, Sutton GM, Pfluger PT, Castaneda TR, Neschen S, Hofmann SM, Howles PN, Morgan DA, Benoit SC, Szanto I, Schrott B, Schürmann A, Joost H-G, Hammond C, Hui DY, Woods SC, Rahmouni K, Butler AA, Farooqi IS, O'Rahilly S, Rohner-Jeanrenaud F, Tschöp MH. The central melanocortin system directly controls peripheral lipid metabolism. *J Clin Invest*. 2007;**117**(11):3475–3488.
27. Martínez de Morentin PB, Whittle AJ, Fernø J, Nogueiras R, Diéguez C, Vidal-Puig A, López M. Nicotine induces negative energy balance through hypothalamic AMP-activated protein kinase. *Diabetes*. 2012;**61**(4):807–817.
28. Martínez de Morentin PB, González-García I, Martins L, Lage R, Fernández-Mallo D, Martínez-Sánchez N, Ruíz-Pino F, Liu J, Morgan DA, Pinilla L, Gallego R, Saha AK, Kalsbeek A, Fliers E, Bisschop PH, Diéguez C, Nogueiras R, Rahmouni K, Tena-Sempere M, López M. Estradiol regulates brown adipose tissue thermogenesis via hypothalamic AMPK. *Cell Metab*. 2014;**20**(1):41–53.
29. Martins L, Seoane-Collazo P, Contreras C, González-García I, Martínez-Sánchez N, González F, Zalvide J, Gallego R, Diéguez C, Nogueiras R, Tena-Sempere M, López M. A functional link between AMPK and orexin mediates the effect of BMP8B on energy balance. *Cell Reports*. 2016;**16**(8):2231–2242.
30. Naldini L, Blömer U, Gage FH, Trono D, Verma IM. Efficient transfer, integration, and sustained long-term expression of the transgene in adult rat brains injected with a lentiviral vector. *Proc Natl Acad Sci USA*. 1996;**93**(21):11382–11388.
31. Nunes PM, van de Weijer T, Veltien A, Arnts H, Hesselink MK, Glatz JF, Schrauwen P, Tack CJ, Heerschap A. Increased intramyocellular lipids but unaltered in vivo mitochondrial oxidative phosphorylation in skeletal muscle of adipose triglyceride lipase-deficient mice. *Am J Physiol Endocrinol Metab*. 2012;**303**(1):E71–E81.
32. Herrero L, Rubí B, Sebastián D, Serra D, Asins G, Maechler P, Prentki M, Hegardt FG. Alteration of the malonyl-CoA/carnitine palmitoyltransferase I interaction in the beta-cell impairs glucose-induced insulin secretion. *Diabetes*. 2005;**54**(2):462–471.
33. Seo S, Ju S, Chung H, Lee D, Park S. Acute effects of glucagon-like peptide-1 on hypothalamic neuropeptide and AMP activated kinase expression in fasted rats. *Endocr J*. 2008;**55**(5):867–874.

34. Minokoshi Y, Alquier T, Furukawa N, Kim Y-B, Lee A, Xue B, Mu J, Foufelle F, Ferré P, Birnbaum MJ, Stuck BJ, Kahn BB. AMP-kinase regulates food intake by responding to hormonal and nutrient signals in the hypothalamus. *Nature*. 2004;**428**(6982):569–574.
35. Cota D, Proulx K, Smith KAB, Kozma SC, Thomas G, Woods SC, Seeley RJ. Hypothalamic mTOR signaling regulates food intake. *Science*. 2006;**312**(5775):927–930.
36. Foster KG, Fingar DC. Mammalian target of rapamycin (mTOR): conducting the cellular signaling symphony. *J Biol Chem*. 2010; **285**(19):14071–14077.
37. Satoh A, Brace CS, Ben-Josef G, West T, Wozniak DF, Holtzman DM, Herzog ED, Imai S. SIRT1 promotes the central adaptive response to diet restriction through activation of the dorsomedial and lateral nuclei of the hypothalamus. *J Neurosci*. 2010;**30**(30):10220–10232.
38. Kang L, Routh VH, Kuzhikandathil EV, Gaspers LD, Levin BE. Physiological and molecular characteristics of rat hypothalamic ventromedial nucleus glucosensing neurons. *Diabetes*. 2004;**53**(3):549–559.
39. Schwinkendorf DR, Tsatsos NG, Gosnell BA, Mashek DG. Effects of central administration of distinct fatty acids on hypothalamic neuropeptide expression and energy metabolism. *Int J Obes*. 2011; **35**(3):336–344.
40. Toda C, Shiuchi T, Lee S, Yamato-Esaki M, Fujino Y, Suzuki A, Okamoto S, Minokoshi Y. Distinct effects of leptin and a melanocortin receptor agonist injected into medial hypothalamic nuclei on glucose uptake in peripheral tissues. *Diabetes*. 2009;**58**(12): 2757–2765.
41. Choi Y-H, Fujikawa T, Lee J, Reuter A, Kim KW. Revisiting the ventral medial nucleus of the hypothalamus: the roles of SF-1 neurons in energy homeostasis. *Front Neurosci*. 2013;**7**:71.
42. López M, Lage R, Saha AK, Perez-Tilve D, Vazquez MJ, Varela L, Sangiao-Alvarellos S, Tovar S, Raghay K, Rodriguez-Cuenca S, Deoliveira RM, Castaneda T, Datta R, Dong JZ, Culler M, Sleeman MW, Alvarez CV, Gallego R, Lelliott CJ, Carling D, Tschop MH, Dieguez C, Vidal-Puig A. Hypothalamic fatty acid metabolism mediates the orexigenic action of ghrelin. *Cell Metab*. 2008;**7**(5): 389–399.
43. Andrews ZB, Liu ZW, Walllingford N, Erion DM, Borok E, Friedman JM, Tschop MH, Shanabrough M, Cline G, Shulman GI, Coppola A, Gao XB, Horvath TL, Diano S. UCP2 mediates ghrelin's action on NPY/AgRP neurons by lowering free radicals. *Nature*. 2008;**454**(7206):846–851.
44. Benani A, Troy S, Carmona MC, Fioramonti X, Lorsignol A, Leloup C, Casteilla L, Penicaud L. Role for mitochondrial reactive oxygen species in brain lipid sensing: redox regulation of food intake. *Diabetes*. 2007;**56**(1):152–160.
45. Pecqueur C, Bui T, Gelly C, Hauchard J, Barbot C, Bouillaud F, Ricquier D, Miroux B, Thompson CB. Uncoupling protein-2 controls proliferation by promoting fatty acid oxidation and limiting glycolysis-derived pyruvate utilization. *FASEB J*. 2008;**22**(1):9–18.
46. Dietrich MO, Horvath TL. Hypothalamic control of energy balance: insights into the role of synaptic plasticity. *Trends Neurosci*. 2013;**36**(2):65–73.
47. Liu T, Kong D, Shah BP, Ye C, Koda S, Saunders A, Ding JB, Yang Z, Sabatini BL, Lowell BB. Fasting activation of AgRP neurons requires NMDA receptors and involves spinogenesis and increased excitatory tone. *Neuron*. 2012;**73**(3):511–522.
48. Yang Y, Atasoy D, Su HH, Sternson SM. Hunger states switch a flip-flop memory circuit via a synaptic AMPK-dependent positive feedback loop. *Cell*. 2011;**146**(6):992–1003.
49. Takahashi KA, Cone RD. Fasting induces a large, leptin-dependent increase in the intrinsic action potential frequency of orexigenic arcuate nucleus neuropeptide Y/Agouti-related protein neurons. *Endocrinology*. 2005;**146**(3):1043–1047.
50. Gratacòs-Batlle E, Yefimenko N, Cascos-García H, Soto D. AMPAR interacting protein CPT1C enhances surface expression of GluA1-containing receptors. *Front Cell Neurosci*. 2014;**8**:469.
51. Schwenk J, Harmel N, Brechet A, Zolles G, Berkefeld H, Müller CS, Bildl W, Baehrens D, Hüber B, Kulik A, Klöcker N, Schulte U, Fakler B. High-resolution proteomics unravel architecture and molecular diversity of native AMPA receptor complexes. *Neuron*. 2012;**74**(4):621–633.
52. Schwenk J, Baehrens D, Haupt A, Bildl W, Boudkkazi S, Roeper J, Fakler B, Schulte U. Regional diversity and developmental dynamics of the AMPA-receptor proteome in the mammalian brain. *Neuron*. 2014;**84**(1):41–54.
53. Fadó R, Soto D, Miñano-Molina AJ, Pozo M, Carrasco P, Yefimenko N, Rodríguez-Álvarez J, Casals N. Novel regulation of the synthesis of α-amino-3-hydroxy-5-methyl-4-isoxazolepropionic acid (AMPA) receptor subunit GluA1 by carnitine palmitoyltransferase 1C (CPT1C) in the hippocampus. *J Biol Chem*. 2015; **290**(42):25548–25560.
54. Sugden MC, Holness MJ. Mechanisms underlying regulation of the expression and activities of the mammalian pyruvate dehydrogenase kinases. *Arch Physiol Biochem*. 2006;**112**(3):139–149.
55. Sugden MC, Kraus A, Harris RA, Holness MJ. Fibre-type specific modification of the activity and regulation of skeletal muscle pyruvate dehydrogenase kinase (PDK) by prolonged starvation and refeeding is associated with targeted regulation of PDK isoenzyme 4 expression. *Biochem J*. 2000;**346**(pt 3):651–657.
56. de Lange P, Moreno M, Silvestri E, Lombardi A, Goglia F, Lanni A. Fuel economy in food-deprived skeletal muscle: signaling pathways and regulatory mechanisms. *FASEB J*. 2007;**21**(13):3431–3441.
57. Galgani J, Ravussin E. Energy metabolism, fuel selection and body weight regulation. *Int. J. Obes.* (Lond). 2008;**32**(suppl 7):S109-119.